ORIGINAL ARTICLE   **Open Access**

Development and Analysis of a Closed-Chain Wheel-Leg Mobile Platform

Chaoran Wei, Yanan Yao[*], Jianxu Wu[*] and Ran Liu

Abstract

Current research concerning legged platforms and wheeled platforms primarily focuses on terrain adaptive capability and speed capability, respectively. Compared with wheeled platforms, legged platforms with a closed-chain mechanism still present deficiencies regarding speed ability. To integrate the advantages of these two types of platforms, a wheel-leg mobile platform with two modes based on a closed-chain mechanism is proposed. First, a closed-chain mechanism that generates a high-knee trajectory in legged mode is designed and analyzed based on kinematic analysis. To improve the platform's obstacle-surmounting performance, the dimensional parameters of the closed-chain mechanism are optimized and the design requirements for the platform's frame are analyzed. In addition, the particular structure of the leg group is designed to realize transformation between legged mode and wheeled mode. The mobility of the constructed platform is calculated through an obstacle-surmounting probability analysis. The performances of the two motion modes are analyzed and compared by conducting dynamic simulations. Finally, experiments are carried out to verify both the theoretical analyses and the prototype performance. This study proposes a new approach to designing wheel-leg platforms with prominent speed ability and mobility based on a closed-chain mechanism.

Keywords: Wheel-leg mobile platform, Closed-chain leg mechanism, High-knee trajectory, Obstacle-surmounting probability

1 Introduction

Wheeled robots, with high moving efficiency, simple structure, and low energy consumption, are often used for high-speed transportation on structured roads. However, unstructured terrain environments are complex and diverse. Natural obstacles like large rocks, deep ravines, and steep slopes can render rolling locomotion ineffective [1–6]. To enhance the obstacle-surmounting capability of wheeled robots for achieving speed capability, some novel wheeled robots have been proposed. A novel wheeled robot [7] that transforms from a circled configuration to a spoke-like legged configuration has been reported that is able to overcome obstacles and move quickly on flat ground. A new category of wheel-leg hybrid robot has been presented [8] that can utilize a larger wheel diameter compared with previous hybrid robots to realize a better ability to overcome obstacles. "Roller-Walker" is a leg-wheel hybrid mobile robot using a passive wheel equipped on the tip of each leg [9]. The passive wheel can be transformed into a sole mode using a rotating ankle roll joint when Roller-Walker walks on rough terrain, thereby improving the terrain adaptability of the robot. Kim et al. proposed a new transformable wheel [10] that can climb over an obstacle three times taller than its wheel radius at a relatively high moving speed. A soft robot composed of soft and flexible materials has been reported [11], demonstrating unique characteristics that cannot be found in a conventional hard robot. Although the wheel radius of this robot is small, it can pass obstacles with dimensions similar to the radius of the wheel.

Compared with wheeled robots, legged robots [12–17] have an advantage in terms of terrain adaptive capability on rough terrain and in unstructured

*Correspondence: yayao@bjtu.edu.cn; 13116343@bjtu.edu.cn
School of Mechanical, Electronic and Control Engineering, Beijing Jiaotong University, Beijing 100044, China

Wei *et al. Chin. J. Mech. Eng.*   (2020) 33:80

Page 2 of 13

environments. They can overcome rough terrain using discrete footholds. According to their structure, these legged robots can be divided into two modes: open-chain linkages [18, 19] and closed-chain linkages [20–24]. The "ANYmal" is constructed with four open-chain legs [25]; it can open the door and take the elevator autonomously, and it can even stand up again by itself after being pushed down. Developed by Boston Dynamics, the Bigdog, which has a total of sixteen motors, is capable of walking and carrying cargo in rugged terrain [26]. With similar structures, the open-chain legged robot with several actuated joints (at least HAA, HFE, and KFE [27] on a single leg) requires multiple motors with high power density and a complex dynamic control system.

To simplify the control program and improve the reliability of legged robots, some studies have been carried out on single-degree-of-freedom (DOF) planar linkages with closed chains. As a classic robot with a closed-chain leg mechanism, the "Strandbeest" is constructed with 8-bar leg mechanisms in a multi-legged mode using different crank phase arrangements [28]. To improve the functionality of legged robots, a novel multi-legged horse-riding simulation vehicle has been designed [29]. The functions of this robot include transportation, rehabilitation, and equine-assisted therapy. However, because of the invariable hardware morphology and the single foot-point trajectory of the one-DOF closed-chain leg mechanism, the speed ability and flexibility are seriously limited.

Therefore, we propose a wheel-leg mobile platform based on a closed-chain mechanism. The linkages of the closed-chain leg mechanism can be used as spokes for wheels. This platform utilizes a structural transformation between legged mode and wheeled mode, where the former is useful for surmounting obstacles on unstructured roads and the latter is employed for fast movement on structured roads.

The remainder of this paper is organized as follows. Section 2 describes the leg mechanism with a high-knee trajectory and discusses the design procedures, including mechanism design, kinematics analysis, dimensional optimization, and the design of the leg mechanism. Section 3 analyzes the layout of the wheel-leg mobile platform and the probability of surmounting obstacles. Then, a series of dynamic simulations of the variable-form platform are constructed to verify the theoretical analysis and the properties of the two modes in Section 4. An experimental system is built to confirm the feasibility of the design in Section 5.

2 Mechanism Design and Analysis

2.1 Legged Mechanism Structure

We are inspired by the "golden wheel spider", which not only can crawl using its legs, but also can roll rapidly by transforming itself into a wheel. With this special function, the spider can dodge attacks by enemies. Accordingly, the closed-chain leg mechanism should satisfy the following requirements: (1) it should include a shank link, which is similar to the shank of a reptile; (2) when the closed-chain leg mechanisms transform into a wheel, the shank link can enclose the thigh link and act as a part of the external contour of the wheel. As shown in Figure 1, the Stephenson III-type satisfies the above-mentioned requirements. The links are specified as the ground link (G), thigh link (L), shank link (F), crank (C), and ternary link (T).

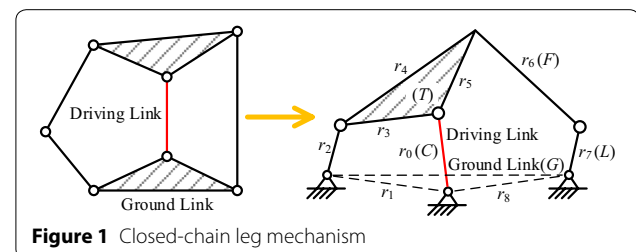### 2.2 Kinematics Analysis and Optimization Design

Based on the Stephenson III-type mechanism mentioned above, the closed-chain leg mechanism was designed as shown in Figure 2. To obtain and optimize the trajectory of the closed-chain foot point, a kinematics analysis was undertaken. The single-leg construction can be decomposed into two loops, and the vector expression of the displacement, velocity, and acceleration of the foot can be obtained through the vector loop method.

The two vector loops are formulized as follows.

$$r_0 + r_1 + r_2 + r_3 = 0, \tag{1}$$

$$r_0 - r_4 - r_6 - r_7 - r_8 = 0. \tag{2}$$

Note that, r_i ($i = 0, 1, ..., 9$) represents the length of the link; θ_i ($i = 0, 1, ..., 9$) represents the angle between r_i and the positive direction of the x-axis ($i = 0, 1, ..., 9$); θ_0 is the input angle of the crank, which varies from 0 to 2π; and ω_i and α_i represent the angular velocity and the angular acceleration, respectively. The unknown variables can be obtained from Eqs. (3)–(5) by solving Eqs. (1) and (2). The intermediate variables are listed in Appendix.

Figure 1 Closed-chain leg mechanism

Wei *et al.* Chin. J. Mech. Eng.   (2020) 33:80

Page 3 of 13

$$\theta_i = \begin{cases} 2\tan^{-1}\left(\dfrac{-b_{i-1}\pm\sqrt{b_{i-1}^2-4a_{i-1}c_{i-1}}}{2a_{i-1}}\right), & i=2,\,3, \\[3mm] 2\tan^{-1}\left(\dfrac{-m_{i-5}\pm\sqrt{m_{i-5}^2-4l_{i-5}n_{i-5}}}{2l_{i-5}}\right), & i=6,\,7, \end{cases} \tag{3}$$

$$\omega_i = \begin{cases} \dfrac{\xi_i}{\xi_1}, & i=2,\,3, \\[3mm] \dfrac{\xi_{i-1}}{\xi_4}, & i=6,\,7, \end{cases} \tag{4}$$

$$\alpha_i = \begin{cases} \dfrac{\rho_i}{\rho_1}, & i=2,\,3, \\[3mm] \dfrac{\rho_{i-1}}{\rho_4}, & i=6,\,7. \end{cases} \tag{5}$$

The numerical solutions can be found using MATLAB^{TM}.

Because point H is the foot point of the leg mechanism, the trajectory of point H can be expressed as follows:

$$-r_0 - r_3 - r_5 + r_9 = r_{10}. \tag{6}$$

The variables θ_{3_5} and θ_{6_9} represent the relative angular relationship between two links. Equation (6) can be decomposed into two-scale equations, as follows:

$$x_H = -r_0\cos\theta_0 - r_3\cos\theta_3 - r_5\cos(\theta_3+\theta_{3\_5}) + r_9\cos(\theta_6-\theta_{6\_9}), \tag{7}$$

$$y_H = -r_0\sin\theta_0 - r_3\sin\theta_3 - r_5\sin(\theta_3+\theta_{3\_5}) + r_9\sin(\theta_6-\theta_{6\_9}). \tag{8}$$

Figure 2 Vector loops

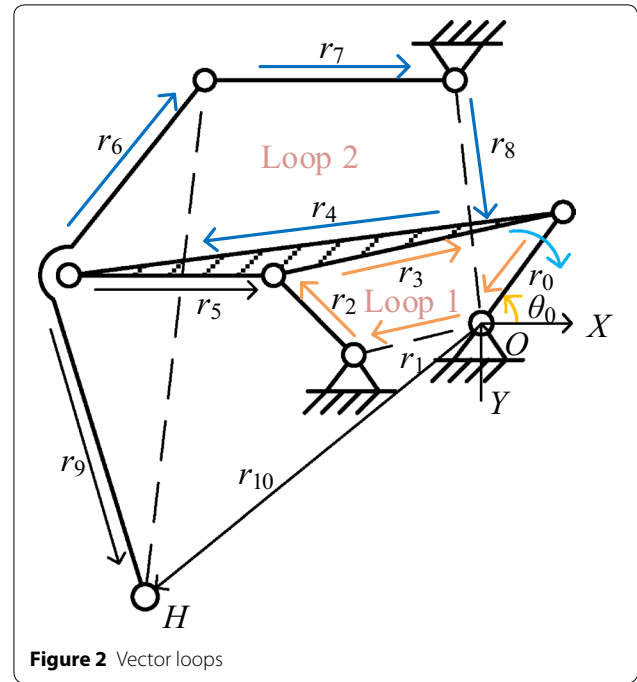The speed and acceleration of point H are shown in Eqs. (9) and (10). Note that $\omega_3=\omega_5$ and $\omega_6=\omega_9$.

To improve the platform's adaptability to unknown terrain in legged mode, the foot trajectory of the leg

$$\begin{bmatrix} v_{xH} \\ v_{yH} \end{bmatrix} = \begin{bmatrix} \dot{x}_H \\ \dot{y}_H \end{bmatrix} = \begin{bmatrix} -r_0\cos\theta_0 & -r_3\cos\theta_3 & -r_5\cos(\theta_3+\theta_{3\_5}) & r_9\cos(\theta_6-\theta_{6\_9}) \\ -r_0\sin\theta_0 & -r_3\sin\theta_3 & -r_5\sin(\theta_3+\theta_{3\_5}) & r_9\sin(\theta_6-\theta_{6\_9}) \end{bmatrix} \begin{bmatrix} \omega_0 \\ \omega_3 \\ \omega_5 \\ \omega_9 \end{bmatrix}, \tag{9}$$

$$\begin{bmatrix} \alpha_{xH} \\ \alpha_{yH} \end{bmatrix} = \begin{bmatrix} \ddot{x}_H \\ \ddot{x}_H \end{bmatrix} = \begin{bmatrix} -r_0\cos\theta_0 & -r_3\cos\theta_3 & -r_5\cos(\theta_3+\theta_{3\_5}) & r_9\cos(\theta_6-\theta_{6\_9}) \\ -r_0\sin\theta_0 & -r_3\sin\theta_3 & -r_5\sin(\theta_3+\theta_{3\_5}) & r_9\sin(\theta_6-\theta_{6\_9}) \end{bmatrix} \begin{bmatrix} 0 \\ \alpha_3 \\ \alpha_5 \\ \alpha_9 \end{bmatrix}$$

$$+ \begin{bmatrix} r_0\sin\theta_0 & r_3\sin\theta_3 & r_5\sin(\theta_3+\theta_{3\_5}) & -r_9\sin(\theta_6-\theta_{6\_9}) \\ -r_0\cos\theta_0 & -r_3\cos\theta_3 & -r_5\cos(\theta_3+\theta_{3\_5}) & r_9\cos(\theta_6-\theta_{6\_9}) \end{bmatrix} \begin{bmatrix} \omega_0^2 \\ \omega_3^2 \\ \omega_5^2 \\ \omega_9^2 \end{bmatrix}. \tag{10}$$

Table 1 Coordinates of pre-assigned points (mm)

i	1	2	3	4	5	6	7	8
$\Delta\theta_0$ (°)	0	45	90	135	180	225	270	315
X_{Hi} (mm)	56	84	62	37	5	12	46	76
Y_{Hi} (mm)	24.3	210	201	59	0	0	0	0

Wei *et al. Chin. J. Mech. Eng.* (2020) 33:80

Page 4 of 13

mechanism should possess obstacle-surmounting capability and load-carrying stability. On a flat road, the walking stability and energy consumption are primarily affected by the straightness of the supporting phase. On an uneven road, the crossing efficiency of the leg mechanism primarily depends on the effective crossing curve height. Accordingly, the goals of this optimization are that the vertical variation during the supporting phase should be as small as possible and the stride height should be as high as possible.

Based on kinematics analysis, the bench trajectory for the initial size can be obtained. The two-dimensional optimization of the initial trajectory can be regarded as a nonlinear optimization problem.

As shown in Table 1, eight pre-assigned points are taken to limit the bench trajectory. In the swing phase, points 1, 2, 3, and 4 limit the width of the phase trajectory. In the supporting phase, points 5, 6, 7, and 8, with the same *y*-coordinate, are used for the supporting straightness.

The maximum approximation of the initial points to the pre-assigned points can be obtained by the objective function shown in Eq. (11):

$$f(x) = \sum_{i=1}^{8} \left[(X_i - X_{Hi})^2 + (Y_i - Y_{Hi})^2 \right]. \quad (11)$$

(X_{Hi}, Y_{Hi}) represents the pre-assigned coordinate points of the bench trajectory. Accordingly, link lengths $(r_0, r_1, \ldots, r_9)$ and link angles $(\theta_1, \theta_{3\_4}, \theta_{4\_5}, \theta_{6\_9}, \theta_8)$ are the variables of the optimization function Eq. (11).
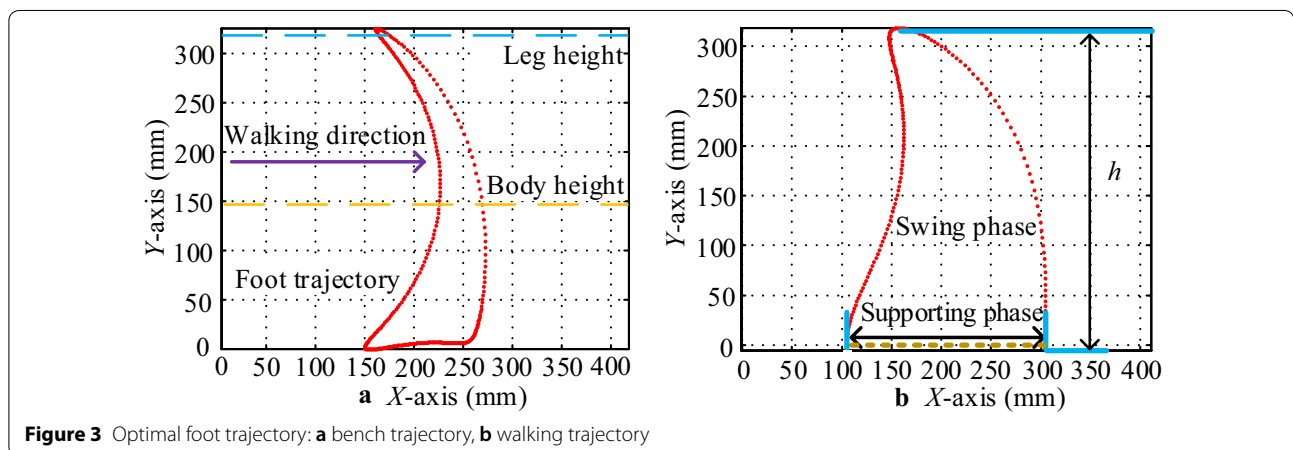
The optimal values of link lengths and link angles are listed in Table 2. The bench trajectory refers to the trajectory generated by the leg mechanism during the bench test, that is, the entire platform does not touch the ground. The walking trajectory refers to the path of the foot point when the platform walks on flat ground in one circle [30]. The bench trajectory and the walking trajectory are shown in Figure 3. The stride height (h) reaches 0.98 times the height of the leg, and is 2.01 times the height of the body. The height for crossing obstacles is thus much higher than that of ordinary legged robots and wheeled robots.

2.3 Mechanism Design

The high-knee trajectory has been obtained through the optimization design. To realize the wheeled mode, the structural parameters should satisfy a particular proportion. Based on kinematic analysis, there is a symmetry construction of the legged mechanism when the crank angle is 0°, and the r_6 link acts a part of the wheel. This symmetry can be obtained through analysis of the legged mechanism: the parameters of l_{OI} and l_{OJ} should be equal to R, and $R = l_{OH}$. In addition, four legs constitute

Table 2 Optimum values of design variables

Design variables	r_0 (mm)	r_1 (mm)	r_2 (mm)	r_3 (mm)	r_6 (mm)	r_7 (mm)
Optimal value	29	57.35	35	56.13	108.8	77
Design variables	r_8 (mm)	r_9 (mm)	θ_1 (rad)	θ_{3_4} (rad)	θ_{6_9} (rad)	θ_8 (rad)
Optimal value	84.12	128.8	−2.88	3.06	2.72	5.71

Figure 3 Optimal foot trajectory: **a** bench trajectory, **b** walking trajectory

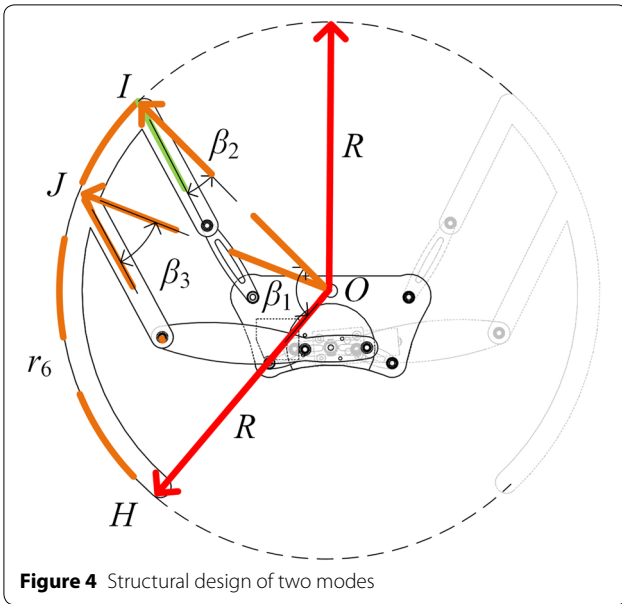Wei *et al. Chin. J. Mech. Eng.* (2020) 33:80

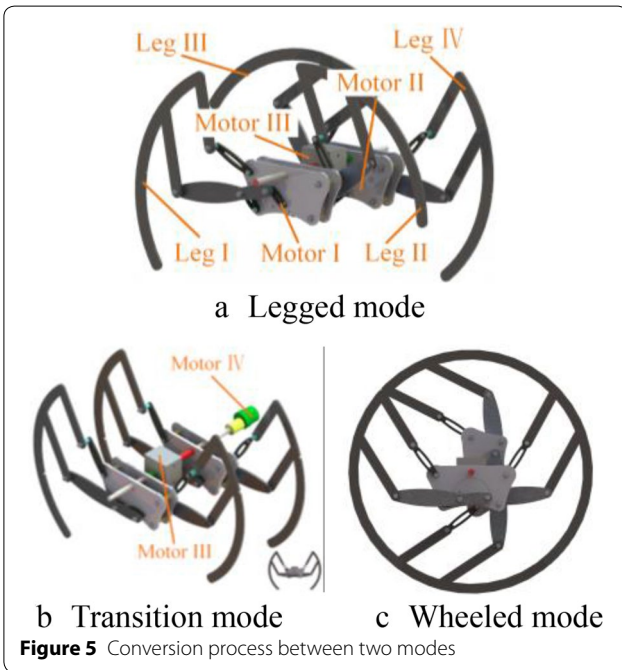Page 5 of 13

Figure 4 Structural design of two modes

Figure 5 Conversion process between two modes

a leg group, or even a wheel when necessary. Therefore, $\beta_1 \geq 90°$ should be guaranteed, and β_2 and β_3 should meet the corresponding dimensional requirements. The structural design is shown in Figure 4.

$$R = \sqrt{\left(x_H^2 + y_H^2\right)}, \qquad (12)$$

Table 3 Phase relations of motors

Motor	Motor I	Motor II	Motor III
Legged mode	θ_0	$\theta_0 + 90°$	$0°$
Wheeled mode	$0°$	$90°$	$90°$
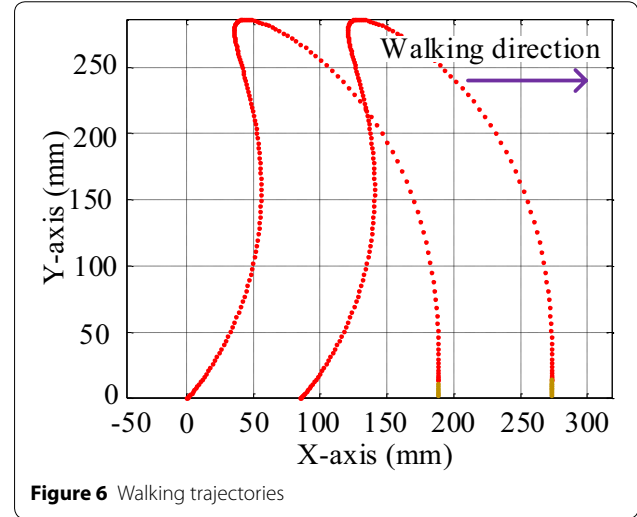
Figure 6 Walking trajectories

$$\beta_1 = \arccos \frac{l_{OI}^2 + l_{OH}^2 - l_{IH}^2}{2 l_{OI} l_{OH}} \geq 90°, \qquad (13)$$

As shown in Figure 5a, the cranks of the closed-chain leg mechanism are respectively powered by motor I and motor II. Leg I and Leg II share one motor, and Leg III and Leg IV adopt the same layout form. The phase difference between the two cranks is 180°. When the platform works on flat roads, the conversion process between the two modes is realized by the following procedures. (1) The crank should be adjusted to the predetermined position ($\theta_0 = 0°$). The transition mode of the leg group is shown in Figure 5b. (2) The angle between Leg I and Leg II should be rotated to 90° by motor III. Then, the transformation between legged mode and wheeled mode can be realized; the wheeled mode is shown in Figure 5c.

The wheels are driven by motor IV, and the angular variation of the motors during the conversion process is shown in Table 3. In addition, θ_0 represents the angle of the crank. When the platform operates on unstructured roads or encounters obstacles, the legged mode of the platform can take advantage of the discrete contacts between the legs and the road. On structured roads, the wheeled mode can fully utilize the ability for efficient movement.
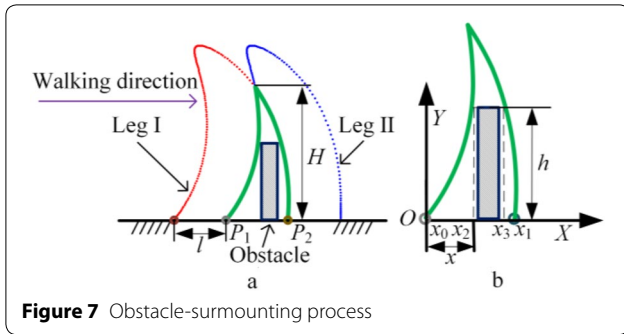
Wei *et al. Chin. J. Mech. Eng.*   (2020) 33:80

Page 6 of 13

Figure 7 Obstacle-surmounting process

3 Obstacle-Surmounting Capability and Frame Size Analysis

3.1 Obstacle-Surmounting Characteristics

Incorporating the structural design of the closed-chain leg mechanism, all links are connected by a rotating pair, and the angle and position of the links are driven by the crank. Because of the geometric invariability of the mechanical system, the motions and trajectories of the links and pairs in an individual mode remain unchanged. The walking trajectories of two feet are shown in Figure 6. To utilize the obstacle-surmounting capability of the walking robot, the relevant parameters of the walking trajectory will play a decisive role.

3.2 Obstacle-Surmounting Probability

Based on analysis of the obstacle-surmounting probability of the closed-chain leg mechanism, Figure 7a illustrates the obstacle-surmounting interval from point P_1 to point P_2. When the foot of Leg I is supported on the ground, the foot of Leg II will fall at point P_1. Then, Leg II is supported on the ground, Leg I starts to surmount the obstacle, and the foot of Leg I falls at point P_2. Finally, Leg II starts to surmount the obstacle, and the closed-chain leg mechanism completes a period of obstacle-surmounting. This is illustrated in Figure 7b, if we do not ignore the width of the obstacle during the analysis. There are always two points, (x_2, 0) and (x_3, 0), satisfying $y(x_2) = y(x_3) = h$ on the curve, when the height of the obstacle is h. In addition, the parameters x_2 and x_3 represent the width of the obstacle in Figure 7b. The x-axis coordinate represents the horizontal displacement, and the y-axis coordinate represents the height of the foot.

In the obstacle-surmounting process, the distance x between the support point P_1 and the obstacle takes a value with equal probability. Value x obeys a uniform distribution in $[x_0,x_1]$, namely $x \sim U[x_0,x_1]$. If the curve of the obstacle-surmounting section can completely wrap the outer contour of the obstacle, the closed-chain leg mechanism will be able to surmount the obstacle

steadily without impact. The corresponding probability density is expressed as Eq. (14):

$$g(x) = \begin{cases} \frac{1}{x_1-x_0}, & x_0 \leq x \leq x_1, \\ 0, & \text{others}. \end{cases} \tag{14}$$

When the obstacle is located in $[x_2,x_3]$, the modular legged unit is able to stride over the barrier with height h. Therefore, the obstacle-surmounting probability of the leg mechanism can be obtained as in Eq. (15):

$$P\{Y \geq h\} = P\{x_2 \leq x \leq x_3\} = \int_{x_2}^{x_3} \frac{1}{x_1-x_0} \mathrm{d}x. \tag{15}$$

Using the least squares method, the fitting process is conducted on discrete points in the x and y data. The achieved fitting function of the obstacle-surmounting curve can be expressed as Eq. (16). In addition, $a = 200.1$, $b = 152$, and $c = 30.69$.

$$y(x) = ae^{\frac{-(x-b)^2}{c^2}}. \tag{16}$$

Using Eq. (16), the inverse function of the fitting function $y(x)$ can be obtained as Eqs. (17) and (18):

$$x_2(y) = b - c\sqrt{\ln H - \ln y}, \tag{17}$$

$$x_3(y) = b + c\sqrt{\ln H - \ln y}. \tag{18}$$

For a certain height $h \in (0, H)$, the obstacle-surmounting probability can be written as follows:

$$P\{Y \geq h\} = \frac{x_3(h) - x_2(h)}{x_1-x_0}. \tag{19}$$

The obstacle height h is defined as $h = H - y'$; then, the evolution of Eq. (19) can be obtained as Eq. (20):

$$F(y') = \begin{cases} 0, & y' \geq H, \\ \frac{2\sqrt{2} \times 21.7 \sqrt{\ln 200.1 - \ln(200.1-y')}}{140}, & 0 \leq y' \leq H, \\ 1, & y' \leq 0. \end{cases} \tag{20}$$

The mathematical expectation of the obstacle width can be obtained, as shown in Eq. (21), so the mathematical expectation of the obstacle height can be obtained as Eq. (22):

Table 4 Minimum distances between foot point and links

Link	r_1	r_2	r_0
Minimum distance (mm)	139.6557	170.5758	215.6814

Wei *et al. Chin. J. Mech. Eng.* (2020) 33:80

Page 7 of 13

$$E(y') = \int_{-\infty}^{+\infty} y' \cdot f(y') \mathrm{d}(y'), \tag{21}$$

$$E(h) = E(H - y') = H - E(y') = 77.6506 \text{ mm.} \tag{22}$$

Based on kinematic analysis, the minimum distance between the foot point and other links of the leg mechanism are listed in Table 4. Utilizing the mathematical expectation, the entire leg mechanism will cross the obstacle successfully without collision.

When the closed-chain leg mechanism climbs a stair, the obstacle-surmounting capability of the legged mode can be better utilized. According to the above analysis, as long as there is only one intersection point between the outer contour of the stair and the obstacle-surmounting curve, in other words, (1) $y(x_2) > h$; (2) $x_3 > x_1$, the platform will be able to climb the stair successfully. Similarly, the distance x between the support point p_1 and the obstacle is a random variable. Therefore, the probability of the closed-chain leg mechanism climbing the stair is shown in Eq. (23):

$$P\{Y \geq h\} = P\{x_2 \leq x \leq x_1\} = \int_{x_2}^{x_1} \frac{1}{x_1 - x_0} \mathrm{d}x. \tag{23}$$

For a certain height $h_1 \in (0, H)$, the obstacle-surmounting probability can be written as Eq. (24):

$$P\{Y \geq h_1\} = \frac{x_1 - x_2(h_1)}{x_1 - x_0}. \tag{24}$$

The obstacle height h_1 is defined as $h_1 = H - y_1'$; then, the evolution of Eq. (24) can be obtained as shown in Eq. (25):

$$F(y_1') = \begin{cases} 0, & y_1' \geq H, \\ \frac{70 + \sqrt{2} \times 21.7\sqrt{\ln 200.1 - \ln(200.1 - y_1')}}{140}, & 0 \leq y_1' \leq H, \\ 1, & y_1' \leq 0. \end{cases} \tag{25}$$

The mathematical expectation of the stair width can be obtained, as shown in Eq. (26), and the mathematical expectation of the stair height is shown in Eq. (27):

$$E(y_1') = \int_{-\infty}^{+\infty} y_1' \cdot f(y_1') \mathrm{d}(y_1'), \tag{26}$$

$$E(h_1) = E(H - y_1') = H - E(y_1') = 138.7753 \text{ mm.} \tag{27}$$

3.3 Layout Form and Frame Size Analysis

In terms of the layout of the wheel-leg mobile platform, from the perspective of increasing the load capacity of the platform, four quad-legged groups are symmetrically
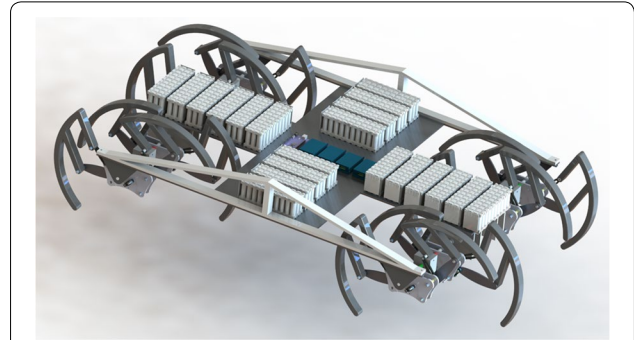

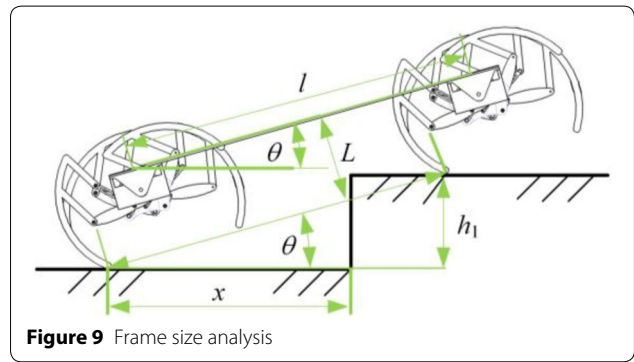**Figure 8** Layout of wheel-leg mobile platform

Figure 9 Frame size analysis

arranged and connected through the frame. Considering the payload capability and the maneuverability of the platform, the two leg groups on the same side should maintain a certain distance when connected with the frame. When the platform works on structured roads, the high-speed capability of the wheeled mode can be fully utilized. The layout of the platform is shown in Figure 8.

When the platform climbs a stair, the front leg steps on the stair, as shown in Figure 9. To climb the stair successfully, the positional relationship between the frame and the outer contour of the stair should be calculated.

Assuming that the distance between the hind leg and the bottom of the obstacle is x, the distance relationship is shown in Eqs. (28) and (29):

$$L \geq (h_1 - x\tan\theta)\cos\theta, \tag{28}$$

$$\sin\theta = \frac{h_1}{l}. \tag{29}$$

The function f is defined as $f = (h_1 - x\sin\theta)\cos\theta$. Obviously, f will take the maximum value when $x = 0$, where the distance between the obstacle and the frame is the maximum value. Therefore, the following two properties can be obtained: (1) $h_1 \leq L/\cos\theta$; (2) $L = 148$ mm. In
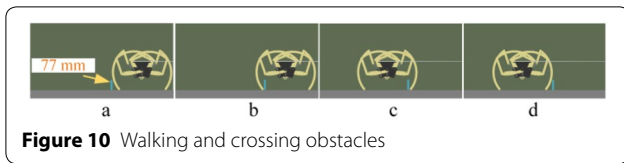
Wei *et al. Chin. J. Mech. Eng.*   (2020) 33:80

Page 8 of 13

Figure 10 Walking and crossing obstacles

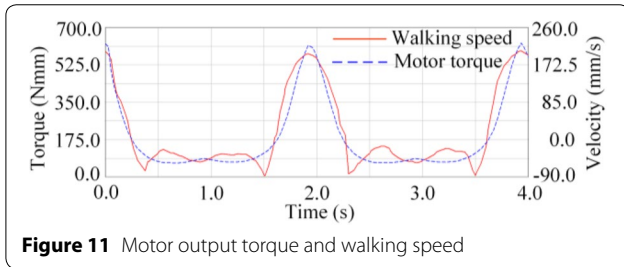**Figure 11** Motor output torque and walking speed
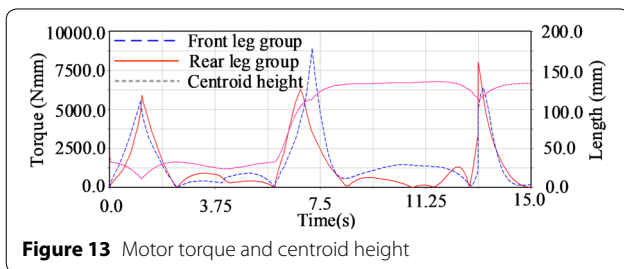

Figure 12 Stair obstacle-surmounting simulation

Figure 13 Motor torque and centroid height

Figure 14 Simulation analysis of climbing slope

Figure 15 Motor output torque

motor is working in wheeled motion. The entire platform was composed of four quad-legged groups, with eight motors in legged mode and four motors in wheeled mode. According to theoretical analysis, the mathematical expectation of the obstacle height was 77 mm. Through the simulation, the process could be obtained where the platform walked on the ground and climbed the obstacle, as shown in Figure 10. In addition, the curves of the motor output torque and the walking speed of the platform are shown in Figure 11.

By analyzing the actual walking trajectory in legged mode, the theoretical maximum height of stair climbing was determined to be 200 mm. As shown in Figure 12, a dynamic simulation of the stair climbing process was carried out. The motor output torque and the centroid height could be obtained during the climbing process, as shown in Figure 13.

The climbing ability of the platform was verified by the simulations shown in Figure 14, where the slope angle was 25°. Here, the frictional force and surface roughness of the slope were not considered.

The steering mode of the wheel-leg mobile platform utilized the speed difference between different side legged groups, which was realized by controlling the crank rotational speeds of different side leg groups. During movement, the contact between the foot and the ground were discontinuous. In addition, the friction between the foot and the ground was a numerous and irregular variable. Therefore, the following assumptions should be set: (1) the platform works on a flat road with good road conditions; (2) a single leg group of the platform is equivalent to one wheel; (3) the centroid of the platform is the symmetric center of the entire platform.

addition, L represents the minimum height of the body. Obviously, the platform can always surmount the obstacle smoothly when $0 \leq h_1 \leq L$. When $L \leq h_1 \leq 200.1$ mm, l should satisfy the following property: $l^2 \leq h_1^4/(h_1^2 - L^2)$. Therefore, as the height of the stair increases, the maximum value of the frame length will be gradually reduced. When the height of the obstacle is 200.1 mm, the maximum length of the frame is $l = 296$ mm.

4 Simulations and Experiments

The entire platform was modeled and analyzed. In one quad-legged group, two motors are working at the same time in legged motion, and only one drive
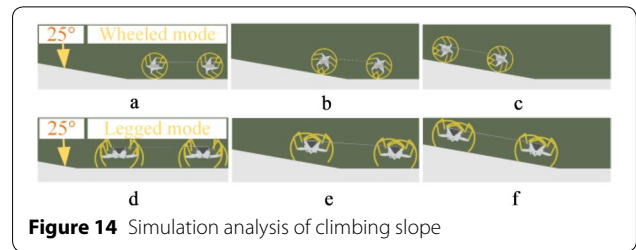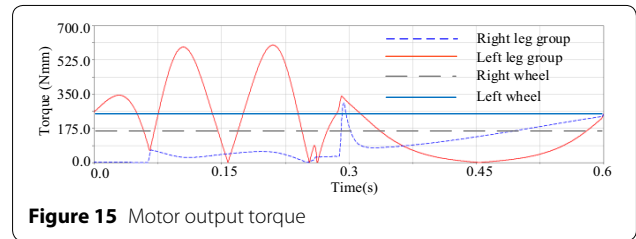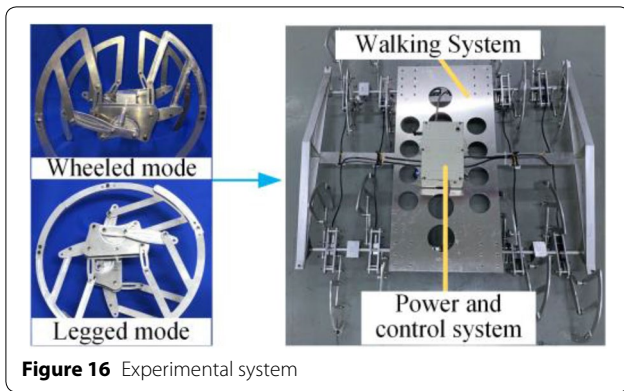
Wei *et al. Chin. J. Mech. Eng.*   (2020) 33:80

Page 9 of 13

Figure 16 Experimental system

and legged mode could be obtained. The motor output torque curve is shown in Figure 15. Comparing different dynamic simulations, the maximum motor torque can be obtained. The maximum torque occurred in the process of climbing the stair, and its value was 8.8 N·mm. Therefore, the motors were selected to satisfy the design requirement with a 1.5-times coefficient of safety. The maximum torque of motor I is therefore 14 N·mm.

5 Prototype and Experiments

As shown in Figure 16, the legged mode and the wheeled mode of the leg groups were assembled. The experimental system is composed of a walking system and a power and control system. The walking system consisted of four

Table 5 Specifications for the platform

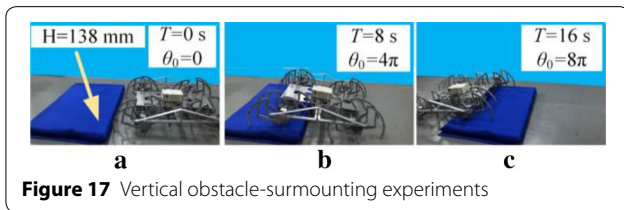| Weight (kg)	Length (mm)	Width (mm)	Height (mm)	Main material
13.5	1500	900	300	Aluminum
Rated voltage (V)	**Rated speed (r/min)**	**Rated speed (r/min)**	**Steering speed (°/s)**	**Frame height (mm)**
24	Motor I: 15	Motor IV: 20	43.8	148

Figure 17 Vertical obstacle-surmounting experiments

The walking speed of the platform is $v = 2k\omega_0/(2\pi)$, where k is the length of the support phase and ω_0 is the angular velocity of the crank. The linear velocity and angular velocity of the centroid during the steering process are $v = (v_L + v_R)/2$ and $\omega = (v_L - v_R)/b$, where b represents the width of the platform and v_L and v_R respectively represent the travel speed of the left and right leg groups. Therefore, the steering radius of the platform is shown in Eq. (30):

$$R = \frac{b}{2} \cdot \frac{\omega_{OR} + \omega_{OL}}{\omega_{OL} - \omega_{OR}}.$$ (30)

As the difference between ω_{OL} and ω_{OR} increases, the steering radius of the platform decreases. When $\omega_{OL} = 5\omega_{OR}$, the steering process was simulated and analyzed, and the motor output torque in both wheeled mode
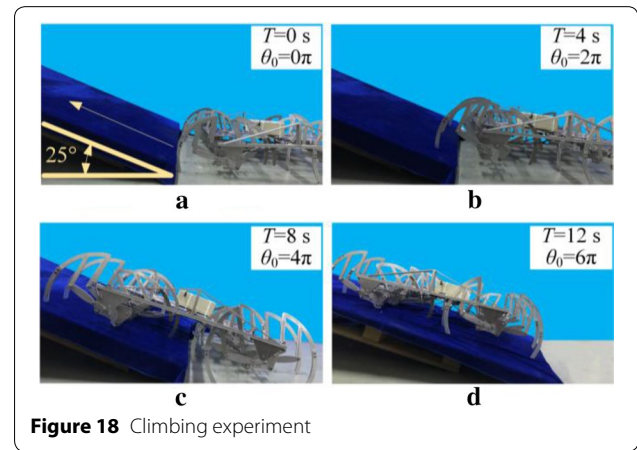

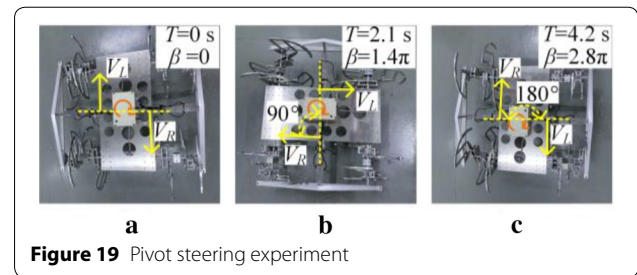**Figure 18** Climbing experiment

Figure 19 Pivot steering experiment

leg groups, and the control system simultaneously controls the four leg groups. The specifications of the platform are listed in Table 5.

According to theoretical analysis, the mathematical expectation of the obstacle-climbing height was 138 mm. Figure 17 shows the stair-climbing experiments, where the obstacle height is 138 mm.

The climbing ability of the wheel-leg mobile platform was verified experimentally with a slope angle of 25°, as shown in Figure 18, where the specific climbing time and the corner of the crank are marked.

In Figure 19, a turning experiment in wheeled mode was performed to validate the feasibility of the experimental system. The left and right wheel mechanisms moved with equal and opposite driving speed (20 r/min), and the platform realized the pivot steering movement. The average steering speed is 43.8°/s. In addition, β represents the driving angle of the motor in wheeled mode.

6 Conclusions

(1) In this paper, a wheel-leg mobile platform was designed that focused on integrating the obstacle-surmounting capability of a closed-chain legged robot with the speed capability of a wheeled robot.

(2) On the basis of kinematics analysis, the optimized parameters and the corresponding foot trajectory of the closed-chain leg mechanism were obtained. The robot's stride height reaches 0.98 times the height of the leg, and is 2.01 times the height of the body.

(3) In the structural design, the transformation between two modes was conducted by employing a special geometric configuration that can realize transformation between legged mode and wheeled mode.

(4) The mobility of the platform in legged mode was evaluated through obstacle-surmounting probability analysis. The mathematical expectation of the obstacle-crossing height is 77.6506 mm, and the mathematical expectation of the stair-climbing height is 138.7753 mm. To optimize the obstacle-surmounting performance of the wheel-leg mobile platform, the design requirements of the frame were analyzed.

(5) A series of virtual experiments were simulated, which confirmed the theoretical analysis. The closed-chain legged mode can enhance the obstacle-surmounting capability; at the same time, the wheeled mode can enhance the mobility of the platform.

Authors' Information
Chaoran Wei, born in 1994, is currently a PhD candidate at *School of Mechanical, Electronic and Control Engineering, Beijing Jiaotong University, China*. He received his master degree from *Beijing Jiaotong University, China,* in 2018. His research interests include mechanisms and mobile robotics.

Yanan Yao, born in 1972, is currently a professor at *School of Mechanical, Electronic and Control Engineering, Beijing Jiaotong University, China*. He received his PhD degree from *Tianjin University, China,* in 1999. His main research interests include mechanisms and mobile robotics.

Jianxu Wu, born in 1989, is currently a PhD candidate at *School of Mechanical, Electronic and Control Engineering, Beijing Jiaotong University, China*. He received his bachelor degree from *Taiyuan University of Science and Technology, China,* in 2012. His main research interests include mechanisms and mobile robotics.

Ran Liu, born in 1991, is currently a PhD candidate at *School of Mechanical, Electronic and Control Engineering, Beijing Jiaotong University, China*. She received her bachelor degree from *Hebei University of Engineering, China*, in 2013. Her research interests include mechanisms and mobile robotics.

Competing Interests
The authors declare no competing financial interests.

Appendix
Angular
Coordinate component of loop 1

$$r_0 \cos \theta_0 + r_1 \cos \theta_1 + r_2 \cos \theta_2 + r_3 \cos \theta_3 = 0 \ ,$$

$$r_0 \sin \theta_0 + r_1 \sin \theta_1 + r_2 \sin \theta_2 + r_3 \sin \theta_3 = 0 \ .$$

Corresponding intermediate variable

$$\eta_1 = r_2,$$

$$\eta_2 = r_3,$$

$$\eta_3 = r_0 \sin \theta_0 + r_1 \sin \theta_1,$$

$$\eta_4 = r_0 \cos \theta_0 + r_1 \cos \theta_1,$$

$$a_1 = \eta_2^2 - \eta_1^2 - \eta_3^2 - \eta_4^2 + 2\eta_1 \eta_4,$$

$$b_1 = -4\eta_1 \eta_3,$$

Wei *et al. Chin. J. Mech. Eng.*   (2020) 33:80

Page 11 of 13

$$c_1 = \eta_2^2 - \eta_1^2 - \eta_3^2 - \eta_4^2 - 2\eta_1\eta_4,$$

$$a_2 = \eta_1^2 - \eta_2^2 - \eta_3^2 - \eta_4^2 + 2\eta_1\eta_4,$$

$$b_2 = -4\eta_2\eta_3,$$

$$c_2 = \eta_1^2 - \eta_2^2 - \eta_3^2 - \eta_4^2 - 2\eta_2\eta_4.$$

Coordinate component of loop 2

$$r_0 \cos\theta_0 - r_4 \cos\theta_4 - r_6 \cos\theta_6 - r_7 \cos\theta_7 - r_8 \cos\theta_8 = 0,$$

$$r_0 \sin\theta_0 - r_4 \sin\theta_4 - r_6 \sin\theta_6 - r_7 \sin\theta_7 - r_8 \sin\theta_8 = 0,$$

$$k_1 \cos\theta_6 + k_2 \cos\theta_7 = k_3,$$

$$k_1 \sin\theta_6 + k_2 \sin\theta_7 = k_4,$$

$$k_1 = r_6,$$

$$k_2 = r_7,$$

$$k_3 = r_0 \cos\theta_0 - r_4 \cos\theta_4 - r_8 \cos\theta_8,$$

$$k_4 = r_0 \sin\theta_0 - r_4 \sin\theta_4 - r_8 \sin\theta_8,$$

$$l_1 = k_2^2 - k_1^2 - k_3^2 - k_4^2 - 2k_1k_3,$$

$$m_1 = 4k_1k_4,$$

$$n_1 = k_2^2 - k_1^2 - k_3^2 - k_4^2 + 2k_1k_3,$$

$$l_2 = k_1^2 - k_2^2 - k_3^2 - k_4^2 - 2k_2k_3,$$

$$m_2 = 4k_2k_4,$$

$$n_2 = k_1^2 - k_2^2 - k_3^2 - k_4^2 + 2k_2k_3.$$

Angular Velocity

Coordinate component of loop 1

$$r_2 \sin\theta_2 \dot\theta_2 + r_3 \sin\theta_3 \dot\theta_3 = -r_0 \sin\theta_0 \dot\theta_0,$$

$$-r_2 \cos\theta_2 \dot\theta_2 - r_3 \cos\theta_3 \dot\theta_3 = r_0 \cos\theta_0 \dot\theta_0,$$

$$\xi_1 = \begin{vmatrix} r_2 \sin\theta_2 & r_3 \sin\theta_3 \\ -r_2 \cos\theta_2 & -r_3 \cos\theta_3 \end{vmatrix},$$

$$\xi_2 = \begin{vmatrix} r_0 \sin\theta_0 \dot\theta_0 & r_3 \sin\theta_3 \\ -r_2 \cos\theta_2 \dot\theta_2 & -r_3 \cos\theta_3 \end{vmatrix},$$

$$\xi_3 = \begin{vmatrix} r_2 \sin\theta_2 & -r_0 \sin\theta_0 \dot\theta_0 \\ -r_2 \cos\theta_2 & r_0 \cos\theta_0 \dot\theta_0 \end{vmatrix}.$$

Coordinate component of loop 2

$$r_6 \sin\theta_6 \dot\theta_6 + r_7 \sin\theta_7 \dot\theta_7 = r_0 \sin\theta_0 \dot\theta_0 - r_4 \sin\theta_4 \dot\theta_4,$$

$$-r_6 \cos\theta_6 \dot\theta_6 - r_7 \cos\theta_7 \dot\theta_7 = -r_0 \cos\theta_0 \dot\theta_0 + r_4 \cos\theta_4 \dot\theta_4,$$

$$\xi_4 = \begin{vmatrix} r_6 \sin\theta_6 & r_7 \sin\theta_7 \\ -r_6 \cos\theta_6 & -r_7 \cos\theta_7 \end{vmatrix},$$

$$\xi_5 = \begin{vmatrix} r_0 \sin\theta_0 \dot\theta_0 - r_4 \sin\theta_4 \dot\theta_4 & r_7 \sin\theta_7 \\ -r_0 \cos\theta_0 \dot\theta_0 + r_4 \cos\theta_4 \dot\theta_4 & -r_7 \cos\theta_7 \end{vmatrix},$$

$$\xi_6 = \begin{vmatrix} r_6 \sin\theta_6 & r_0 \sin\theta_0 \dot\theta_0 - r_4 \sin\theta_4 \dot\theta_4 \\ -r_6 \cos\theta_6 & -r_0 \cos\theta_0 \dot\theta_0 + r_4 \cos\theta_4 \dot\theta_4 \end{vmatrix}.$$

Angular Acceleration

Coordinate component of loop 1

$$r_2 \sin\theta_2 \alpha_2 + r_3 \sin\theta_3 \alpha_3 = -r_0 \cos\theta_0 \omega_0^2 - r_2 \cos\theta_2 \omega_2^2 - r_3 \cos\theta_3 \omega_3^2,$$

$$-r_2 \cos\theta_2 \alpha_2 - r_3 \cos\theta_3 \alpha_3 = -r_0 \sin\theta_0 \omega_0^2 - r_2 \sin\theta_2 \omega_2^2 - r_3 \sin\theta_3 \omega_3^2,$$

Wei *et al. Chin. J. Mech. Eng.*   (2020) 33:80

Page 12 of 13

$$x_1 = r_2 \sin\theta_2\alpha_2,$$

$$y_1 = r_3 \sin\theta_3\alpha_3,$$

$$z_1 = -r_0 \cos\theta_0\omega_0^2 - r_2 \cos\theta_2\omega_2^2 - r_3 \cos\theta_3\omega_3^2,$$

$$x_2 = -r_2 \cos\theta_2\alpha_2,$$

$$y_2 = -r_3 \cos\theta_3\alpha_3,$$

$$z_2 = -r_0 \sin\theta_0\omega_0^2 - r_2 \sin\theta_2\omega_2^2 - r_3 \sin\theta_3\omega_3^2,$$

$$\rho_1 = \begin{vmatrix} x_1 & y_1 \\ x_2 & y_2 \end{vmatrix},$$

$$\rho_2 = \begin{vmatrix} z_1 & y_1 \\ z_2 & y_2 \end{vmatrix},$$

$$\sigma_1 = \begin{vmatrix} x_1 & z_1 \\ x_2 & z_2 \end{vmatrix}.$$

Coordinate component of loop 2

$$r_6 \sin\theta_6\alpha_6 + r_7 \sin\theta_7\alpha_7 = r_0 \cos\theta_0\omega_0^2 - r_4 \sin\theta_4\alpha_4$$
$$-r_4 \cos\theta_4\omega_4^2 - r_6 \cos\theta_6\omega_6^2 - r_7 \cos\theta_7\omega_7^2,$$

$$-r_6 \cos\theta_6\alpha_6 - r_7 \cos\theta_7\alpha_7 = r_0 \sin\theta_0\omega_0^2 + r_4 \cos\theta_4\alpha_4$$
$$-r_4 \sin\theta_4\omega_4^2 - r_6 \sin\theta_6\omega_6^2 - r_7 \sin\theta_7\omega_7^2,$$

$$x_3 = r_6 \sin\theta_6\alpha_6,$$

$$y_3 = r_7 \sin\theta_7\alpha_7,$$

$$z_3 = r_0 \cos\theta_0\omega_0^2 - r_4 \sin\theta_4\alpha_4 - r_4 \cos\theta_4\omega_4^2$$
$$- r_6 \cos\theta_6\omega_6^2 - r_7 \cos\theta_7\omega_7^2,$$

$$x_4 = -r_6 \cos\theta_6\alpha_6,$$

$$y_4 = -r_7 \cos\theta_7\alpha_7,$$

$$z_4 = r_0 \sin\theta_0\omega_7^2 + r_4 \cos\theta_4\alpha_4 - r_4 \sin\theta_4\omega_4^2$$
$$-r_6 \sin\theta_6\omega_6^2 - r_7 \sin\theta_7\omega_7^2,$$

$$\rho_4 = \begin{vmatrix} x_3 & y_3 \\ x_4 & y_4 \end{vmatrix},$$

$$\rho_5 = \begin{vmatrix} z_3 & y_3 \\ z_4 & y_4 \end{vmatrix},$$

$$\rho_6 = \begin{vmatrix} x_3 & z_3 \\ x_4 & z_4 \end{vmatrix}.$$

References
[1]   W H Chen, H S Lin, Y M Lin, et al. TurboQuad: A novel leg–wheel transformable robot with smooth and fast behavioral transitions. *IEEE Transactions on Robotics*, 2017, 33(5): 1025–1040.
[2]   F J Comin, W A Lewinger, C M Saaj, et al. Trafficability assessment of deformable terrain through hybrid wheel-leg sinkage detection. *Journal of Field Robotics*, 2017, 34(3): 451–476.
[3]   Y X Xin, X W Rong, Y B Li, et al. Movements and balance control of a wheel-leg robot based on uncertainty and disturbance estimation method. *IEEE Access*, 2019, 7: 133265–133273.
[4]   Y X Xin, H Chai, Y B Li, et al. Speed and acceleration control for a two wheel-leg robot based on distributed dynamic model and whole-body control. *IEEE Access*, 2019, 7: 180630–180639.
[5]   F J Comin, C M Saaj. Models for slip estimation and soft terrain characterization with multilegged wheel-legs. *IEEE Transactions on Robotics*, 2017, 33(6): 1438–1452.
[6]   F L Zhou, X J Xu, H J Xu, et al. Transition mechanism design of a hybrid wheel-track-leg based on foldable rims. *Proceedings of the Institution of Mechanical Engineers, Part C: Journal of Mechanical Engineering Science*, 2019, 233(13): 4788–4801.
[7]   Y She, C J Hurd, H J Su. A transformable wheel robot with a passive leg. *IEEE/RSJ International Conference on Intelligent Robots and Systems*, Hamburg, Germany, Sept. 28–Oct. 2, 2015: 4165–4170.
[8]   K Tadakuma, R Tadakuma, A Maruyama, et al. Mechanical design of the wheel-leg hybrid mobile robot to realize a large wheel diameter. *IEEE/RSJ International Conference on Intelligent Robots and Systems*, Taipei, Taiwan, China, October 18–22, 2010: 3358–3365.
[9]   G Endo, H Shigeo. Study on roller-walker-energy efficiency of roller-walk. *IEEE International Conference on Robotics and Automation*, Shanghai, China, May 9–13, 2011: 5050–5055.
[10]   Y S Kim, K J Cho, C N Chu. Wheel transformer: A wheel-leg hybrid robot with passive transformable wheels. *IEEE Transactions on Robotics*, 2014, 30(6): 1487–1498.
[11]   D Y Lee, J S Koh, J S Kim, et al. Deformable-wheel robot based on soft material. *International Journal of Precision Engineering and Manufacturing*, 2013, 14(8): 1439–1445.
[12]   G Chen, B Jin, Y Chen. Nonsingular fast terminal sliding mode posture control for six-legged walking robots with redundant actuation. *Mechatronics*, 2018, 50: 1–15.
[13]   C Hubicki, J Grimes, M Jones, et al. Atrias: Design and validation of a tether-free 3d-capable spring-mass bipedal robot. *The International Journal of Robotics Research*, 2016, 35(12): 1497–1521.
[14]   C Hubicki, A Abate, P Clary, et al. Walking and running with passive compliance. *IEEE Robotics and Automation Magazine*, 2016: 4–1.
[15]   M Schwarz, T Rodehutskors, D Droeschel, et al. NimbRo Rescue: Solving disaster-response tasks through mobile manipulation robot Momaro. *Journal of Field Robotics*, 2017, 34(2): 400–425.
[16]   D Belter, M R Nowicki. Optimization-based legged odometry and sensor fusion for legged robot continuous localization. *Robotics and Autonomous Systems*, 2019, 111: 110–124.
[17]   T Matsuzawa, A Koizumi, K Hashimoto, et al. Crawling gait for four-limbed robot and simulation on uneven terrain. *IEEE-RAS International Conference on Humanoid Robots*, Cancun, Mexico, Nov 15–17, 2016: 1270–1275.

[18] R Buchanan, T Bandyopadhyay, M Bjelonic, et al. Walking posture adaptation for legged robot navigation in confined spaces. *IEEE Robotics and Automation Letters*, 2019, 4(2): 2148-2155.

[19] K Jayaram, R J Full. Cockroaches traverse crevices, crawl rapidly in confined spaces, and inspire a soft, legged robot. *Proceedings of the National Academy of Sciences*, 2016, 113(8): E950-E957.

[20] J K Sheba, M R Elara, E Martínez-García, et al. Trajectory generation and stability analysis for reconfigurable Klann mechanism based walking robot. *Robotics*, 2016, 5(3): 13.

[21] S Nansai, M R Elara, M Iwase. Speed control of Jansen linkage mechanism for exquisite tasks. *Journal of Advanced Simulation in Science and Engineering*, 2016, 3(1): 47–57.

[22] H B Zang, L G Shen. Research and optimization design of mechanism for Theo Jansen bionic leg. *Journal of Mechanical Engineering*, 2017, 53(15): 101-109. (in Chinese)

[23] J X Wu, Q Ruan, Y A Yao. A novel skid-steering walking vehicle with dual single-driven quadruped mechanism. *Mechanisms, Transmissions and Application*, Springer, Cham, 2015: 231–238.

[24] J X Wu, Y A Yao, Q Ruan, et al. Design and optimization of a dual quadruped vehicle based on whole close-chain mechanism. *Proceedings of the Institution of Mechanical Engineers, Part C: Journal of Mechanical Engineering Science*, 2017, 231(19): 3601–3613.

[25] M Hutter, C Gehring, A Lauber, et al. Anymal-toward legged robots for harsh environments. *Advanced Robotics*, 2017, 31(17): 918–931.

[26] M Raibert, K Blankespoor, G Nelson. Bigdog, the rough-terrain quadruped robot. *Proceedings of the IFAC World Congress*, Seoul, Republic of Korea, 2008, 41(2): 10822–10825.

[27] J Hwangbo, J Lee. Learning agile and dynamic motor skills for legged robots. *Science Robotics*, 2019, 4(26): 5872.

[28] D Giesbrecht, C Q Wu, N Sepehri. Design and optimization of an eight bar legged walking mechanism imitating a kinetic sculpture, "Wind Beast". *Transactions of the Canadian Society for Mechanical Engineering*, 2012, 36(4): 343–355.

[29] J X Wu, Y A Yao. Design and analysis of a novel multi-legged horse-riding simulation vehicle for equine-assisted therapy. *Proceedings of the Institution of Mechanical Engineers, Part C: Journal of Mechanical Engineering Science*, 2018, 232(16): 2912–2925.

[30] J X Wu, Y A Yao. Design and analysis of a novel walking vehicle based on leg mechanism with variable topologies. *Mechanism and Machine Theory*, 2018, 128: 663–681.